

Peculiarities of amplitude and phase spectra of semiconductor structures in THz frequency range

Yu.M. Lyaschuk^{1,*}, V.V. Korotyeyev^{1,2,**}, V.A. Kochelap¹

¹*V. Lashkaryov Institute of Semiconductor Physics, NAS of Ukraine, Department of Theoretical Physics 41, prospect Nauky, 03680 Kyiv, Ukraine*

²*Center for Physical Sciences and Technology, Sauletekio al. 3, LT-10257 Vilnius, Lithuania*
E-mail: yulashchuk@gmail.com* ; koroteev@ukr.net**

Abstract. We have reviewed main peculiarities of amplitude and phase transmission/reflection spectra of different model semiconductor structures, including bare dielectric substrate, thin conductive layer placed between two dielectric media, thin conductive layer on dielectric substrate and hybrid plasmonic structures with thin conductive layer under metallic grating. The analysis has been performed using the analytical expressions obtained as a result of solving the Maxwell equations at normal incidence of plane electromagnetic waves. We have shown that specific behavior of the amplitude and phase spectra in THz frequency range can be used to determine basic electric parameters of electron gas, including electron concentration and electron mobility, in the framework of advanced THz time-domain measurements. Finally, we proposed efficient, electrically-controllable THz phase modulator based on effect of two-dimensional plasmon resonances in hybrid plasmonic structure with a spatially modulated electron concentration in a thin conductive layer.

Keywords: phase, phase spectra, THz time-domain spectroscopy, THz phase modulator, plasmonic structure, metallic grating.

<https://doi.org/10.15407/spqeo25.02.121>
PACS 07.57.-c, 42.25.Bs, 42.79.Pw, 85.60.-q

Manuscript received 25.12.21; revised version received 17.02.22; accepted for publication 22.06.22; published online 30.06.22.

1. Introduction

Currently, for spectroscopy of different materials in sub- and THz frequency range two well-developed techniques are widely used: THz-time-domain spectroscopy (THz-TDS) and Fourier transform far-infrared spectroscopy (FTIR). THz-TDS is based on the direct time-domain sampling with ultrafast-laser pump/probe configuration. Particularly, broadband THz radiation is generated in the form of picosecond pulses under fast excitation of a photoconductive switch [1–3] or a surface emitter [4] excited by the femtosecond laser. The shape of the picosecond transients transmitted/reflected through/from the sample can be recorded using photo-conductive or electro-optical sampling schemes [5]. Both schemes are sensitive to the electric field of the emitted pulses in time domain. The Fast-Fourier transformation of the obtained electric field traces provides access to both amplitude and phase spectra in the frequency domain. The modern THz-TDS systems utilizing the femtosecond fiber lasers and LT-GaAs photo-conductive antenna are relatively compact setups with possibility of measurements in the frequency range of 0.1...5 THz.

In contrast to THz-TDS, advanced FTIR spectrometers are cumbersome setup and perform measurements indirectly in the time domain *via* interferometry of the black-body radiation emitted by global. FTIR spectroscopy works well at the higher frequency, typically, it covers the spectral range from 2 THz up to the near-infrared frequencies. The FTIR systems can be adapted for measuring both transmission/reflection and emission spectra [6–8].

However, FTIR as well as other well-established spectroscopic and THz imaging systems based on continuous wave tunable electronic sources [9, 10] and quadratic detectors, such as bolometer [11, 12], field-effect transistors [13], Schottky [14] or bow-tie [15] diodes cannot be applied for measuring the phase spectra. The knowledge of the phase spectra is crucially important for extraction of dielectric properties (index of refraction and absorption coefficient), as well as for some applications, it can be achieved in THz-TDS measurements.

After the first demonstration and discussion of the basic principles inherent to pump-probe measurements, dated by 1989 [16], the TD spectroscopy experienced

a great improvement and nowadays becomes important tool for express analysis of different semiconductor materials [17–20]. Moreover, the generation of high-field pulses with a maximum peak of the electric field of 100...300 kV/cm [21] opens excellent perspectives for high-field THz-TD spectroscopy and study of strongly-nonequilibrium dynamics of the carriers [22–24]. Recently, THz-TD spectroscopy was applied to investigations of resonant properties of hybrid plasmonic structures with two-dimensional electron gas [25–29]. These structures are in focus of current THz applications [30], including electrically driven emitters [7, 8, 31], detectors [32–34] and modulator [35] of THz radiation. Also, they are very promising for fundamental investigations of 2D plasmon instabilities under the grating [36–39].

Nevertheless, the phase retrieval from THz time-domain measurements and correct reconstruction of the basic parameters is not trivial problem [40, 41], especially for the case of THz-transparent plasmonic structures with multi-layered geometry. The aim of this paper is to provide theoretical analysis of main peculiarities inherent to the phase spectra in both transmission and reflection geometry as well as their correlations with the features in the amplitude spectra for several model structures with a thin conductive layer, including grating-based plasmonic structures. Below, the conductive layer will be considered as delta-thin, *i.e.* this layer will be described by two-dimensional parameters. Such assumption is valid when the layer thickness is much less than the wavelength of an incident electro-magnetic wave.

We will show that some features in the phase spectra can serve for unambiguous determination of important parameters of the conductive layer, namely: electron concentrations, scattering time and mobility at high frequencies. We will discuss the possibility of the fast electrical control of the phase shift by the grating-gated conductive layer in regime of the plasmon resonance. The latter can be important for the different photonic application, such as THz wave front control, manipulation of polarization, THz imaging, THz digital holography, *etc.* [42, 43].

The paper is organized as follows. In Section 2, we systemize analytical expressions and perform analysis of both amplitude and phase transmission/reflection for model non-resonant structures: a single dielectric substrate, the conductive layer on the interface between two half-spaces, the conductive layer on a substrate. The resonant structure such as the conductive layer under the grating is analyzed in Section 3. In Section 4, we performed numerical simulation of the phase and power spectra for the grating-gated plasmonic structure with spatially modulated electron concentration of the conductive layer. Main conclusions are summarized in Section 5.

2. Non-resonant structures

Usually, the electrodynamic response of an investigated structure is formulated as response on plane electromagnetic (*em*) wave, $E_i = E_0(\omega) \exp(i\phi_i(\vec{\rho}, t))$,

with amplitude E_0 and phase $\phi_i(\vec{\rho}, t) = i\vec{k}_i\vec{\rho} - i\omega\tau$, where $|\vec{k}_i| = \omega\sqrt{\varepsilon_i}/c$, $\vec{\rho}$ is the coordinate vector, ω is the frequency, c is the light velocity in vacuum and ε_i is dielectric permittivity of the ambient medium. General solution of the Maxwell equations contains the transmitted/reflected waves, $E_{t,r}(\vec{\rho}, t) = E_{t,r}(\omega) \exp(i\phi_j(\vec{\rho}, t))$ with complex-valued amplitudes $E_{t,r}(\omega) = |E_{t,r}(\omega)| \exp(i\phi_{t,r}(\omega))$. Complex valued transmission, $t(\omega)$, and reflection, $r(\omega)$, coefficients can be defined as the ratios:

$$\{t, r\}(\omega) = \frac{E_{t,r}(\omega)}{E_i(\omega)} = \frac{|E_{t,r}(\omega)|}{|E_0(\omega)|} \exp(i\phi_{t,r}). \quad (1)$$

These coefficients define the power and phase transmission/reflection spectra and the phase:

$$\{T, R\}(\omega) = |\{t, r\}(\omega)|^2; \quad \varphi_{t,r}(\omega) = \text{Arg}[\{t, r\}(\omega)]. \quad (2)$$

The designation $\text{Arg}[z]$ stands for the argument of the complex number, $z = x + iy$ and can be defined as follows:

$$\text{Arg}[x + iy] = \begin{cases} \arctan(y/x), & \text{if } x > 0 \\ \arctan(y/x) + \pi \text{sign}(y), & \text{if } x < 0 \\ \pi/2 \text{sign}(y), & \text{if } x = 0 \end{cases} \quad (3)$$

where $\text{sign}(y)$ is the signum function. According definition (3), function $\text{Arg}(z)$ returns the phase value in the interval $[-\pi \dots \pi]$.

Note, $\varphi_t(\omega)$ describes the phase shift between the transmitted wave through the sample and the plane wave propagating at the absence of the sample under the assumption that both waves are recorded in the same spatial point. This condition is realized in THz-TDS setup configuration in the transmission geometry, when time traces of the *reference* signal (recorded without sample) and the *sample* signal (recorded with sample) are measured without changing the optical alignment. In the reflection geometry, $\varphi_r(\omega)$ has a sense of the phase shift between wave the reflected from the sample and the wave reflected from the ideal mirror.

2.1. Substrate

We start our analysis from the simplest case of non-absorbing dielectric plate with the scalar dielectric permittivity, ε_s , and the thickness, D_s . This plate is the constitutive element of many heterostructured samples, and it plays a role of the substrate. For example, sapphire (Al_2O_3) or silicon-carbide (SiC) plates are widely used as substrates in growth processes of $\text{AlGaIn}/\text{GaIn}$ heterostructures. Particularly, a considerable attention is paid to group-III nitrides structures on SiC substrates due to their great potential in high-power electronics. In sub-THz and few-THz frequency ranges, both materials exhibit weak frequency dispersion of ε_s with small optical losses

($\text{Re}[\varepsilon_1] \gg \text{Im}[\varepsilon_1]$) [44]. However, due to the fact that typical substrate thickness is comparable with the wavelength of THz electromagnetic wave, its affect on transmission and reflection spectra is crucial and leads to the emergence of Fabry–Perot fringes in the power transmission/reflection spectra. As can be seen below, some peculiarities relating to the effect of Fabry–Perot fringes also exist in the phase transmission/reflection spectra.

The solution of Maxwell equations at normal incidence provides the following complex-valued transmission, t , and reflection, r , coefficients:

$$t(\Psi_s) = \frac{\exp(-i\Psi_0)}{\cos(\Psi_s) - i\alpha^+ \sin(\Psi_s)}, \quad (4)$$

$$r(\Psi_s) = \frac{i\alpha^- \sin(\Psi_s)}{\cos(\Psi_s) - i\alpha^+ \sin(\Psi_s)}, \quad (5)$$

where $\Psi_{\{s,0\}} = \sqrt{\varepsilon_{\{s,0\}}} \omega D_s / c$ denote dimensionless frequencies. We introduced effective dielectric permittivities $\alpha^\pm = \frac{\varepsilon_s \pm \varepsilon_0}{2\sqrt{\varepsilon_s \varepsilon_0}}$, where ε_0 is the dielectric permittivity of the surrounding. Then, power transmission, T , and power reflection, R , coefficients read as:

$$T(\Psi_s) = \frac{1}{1 + (\alpha^-)^2 \sin^2(\Psi_s)}, \quad (6)$$

$$R(\Psi_s) = (\alpha^-)^2 \sin^2(\Psi_s) T(\Psi_s),$$

where we used that $(\alpha^+)^2 = (\alpha^-)^2 + 1$. The phase transmission coefficient, φ_t , and the phase reflection coefficient, φ_r , can be expressed in the forms of piecewise functions:

$$\begin{aligned} \varphi_t(\Psi_s) &= -\Psi_0 + \text{Arg}[\cos(\Psi_s) + i\alpha^+ \sin(\Psi_s)] = \\ &= -\Psi_0 + \begin{cases} \arctan(\alpha^+ \tan(\Psi_s)), & \Psi_s \in [0, \frac{\pi}{2}] \\ \pi - \arctan(\alpha^+ |\tan(\Psi_s)|), & \Psi_s \in [\frac{\pi}{2}, \pi] \\ -\pi + \arctan(\alpha^+ |\tan(\Psi_s)|), & \Psi_s \in [\pi, \frac{3\pi}{2}] \\ -\arctan(\alpha^+ |\tan(\Psi_s)|), & \Psi_s \in [\frac{3\pi}{2}, 2\pi] \end{cases} \quad (7) \end{aligned}$$

$$\begin{aligned} \varphi_r(\Psi_s) &= \text{Arg}[i \sin(\Psi_s) (\cos(\Psi_s) + i\alpha^+ \sin(\Psi_s))] = \\ &= \begin{cases} \varphi_t(\Psi_s) + \frac{\pi}{2} + \Psi_0, & \Psi_s \in [0, \pi] \\ \varphi_t(\Psi_s) + \frac{3\pi}{2} + \Psi_0, & \Psi_s \in [\pi, 2\pi] \end{cases} \quad (8) \end{aligned}$$

The phase transmission and reflection coefficients are obtained using properties of the complex numbers, *i.e.*, argument of the product of complex numbers is equal to the sum of their arguments.

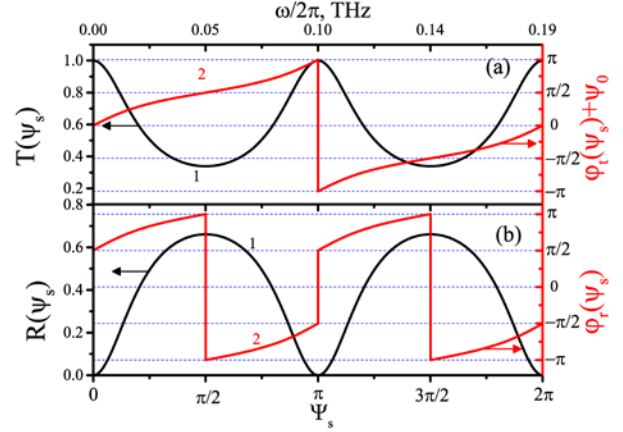


Fig. 1. Power (black lines 1) and phase (red lines 2) transmission (panel (a)) and reflection (panel (b)) coefficients as functions of Ψ_s . Curves are shown for $\varepsilon_s = 9.7$ (SiC) and $\varepsilon_0 = 1$ (vacuum). Parameters α^\pm are equal to 1.7 and 1.4, respectively. The upper axis is rescaled according to the thickness of the substrate $D_s = 500 \mu\text{m}$.

The typical forms of the power and phase (reduced to the interval $[-\pi, \pi]$) spectra of dielectric plate are shown in Fig. 1. Note, the phase transmission spectrum is shown here in terms of the reduced phase, $\bar{\varphi}_t(\Psi_s) = \varphi_t(\Psi_s) + \Psi_0$.

As follows from Eqs (6) to (8), the power coefficients, as well as φ_r , are periodic functions with respect to Ψ_s with the period of π . The phase transmission coefficient, φ_t , has the period of 2π . The functions $T(\Psi_s)$ and $R(\Psi_s)$ reach maximal value, $T_{\max} = 1$, and minimal value of $R_{\min} = 0$, respectively, at the points $\Psi_s = \pi k$ ($k = 0, 1, \dots$). It corresponds to the cases of half-wave plates, $D_s = \lambda_s / 2 \times k$, where $\lambda_s = 2\pi / k_0 \varepsilon_s$ is the wavelength of *em* wave in the medium with dielectric permittivity ε_s . The minimal transmissivity, $T_{\min} = 1 / (1 + (\alpha^-)^2)$, and maximal reflectivity, $R_{\max} = (\alpha^-)^2 / (1 + (\alpha^-)^2)$, are realized for the cases of quarter-wave plates, $\Psi_s = \pi/2 + \pi k$ or $D_s = \lambda_s / 4 \times (2k + 1)$. Note that minimal/maximal values of the transmissivity/reflectivity depend on only effective dielectric permittivity α^- . The latter can be used for determination of ε_s from experimental spectra without knowledge of the geometrical thickness of substrate. Indeed,

$$\alpha^- = \sqrt{\frac{1 - T_{\min}}{T_{\min}}} \quad \text{and} \quad (9)$$

$$\varepsilon_s = \varepsilon_0 T_{\min} \left[1 + \sqrt{1 - T_{\min}^{-2}} \right],$$

$$\text{where } T_{\min} = (2 - T_{\min}) / T_{\min}.$$

In the selected representation, the phase spectra (see red curves in Fig. 1) are the discontinuous functions. Particularly, at the points $\Psi_s = \pi + 2\pi k$, the reduced phase $\bar{\varphi}_t$ has the offsets by 2π . At the same time, φ_r has offsets by 2π at the points $\Psi_s = \pi/2 + \pi k$ and offsets by π at the points $\Psi_s = \pi k$. All offsets by 2π have no physical sense and can be removed in the representation of *unwrapped* phase [41]. In this representation,

$$\begin{aligned} \varphi_t^{umw}(\Psi_s) &= \bar{\varphi}_t(\Psi_s) + 2\pi k - \sqrt{\frac{\varepsilon_0}{\varepsilon_s}} \Psi_s, \\ \text{for } \Psi_s &\in [(2k-1)\pi, (2k+1)\pi], \\ \varphi_r^{umw}(\Psi_s) &= \varphi_r(\Psi_s) + 2\pi k, \\ \text{for } \Psi_s &\in \left[(2k-1)\frac{\pi}{2}, (2k+1)\frac{\pi}{2} \right], \end{aligned} \quad (10)$$

where we used that $\Psi_0 = \sqrt{\varepsilon_0/\varepsilon_s} \Psi_s$. The spectra for unwrapped phases given by Eqs (10) are shown in Fig. 2.

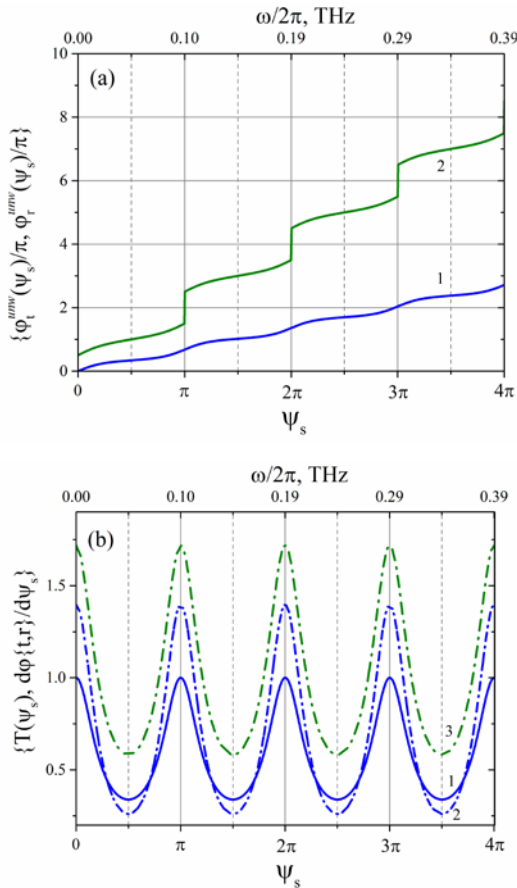


Fig. 2. Panel (a): The phase transmission (blue line 1) and phase reflection (green line 2) coefficients in the representation of the unwrapped phase. Panel (b): derivatives of the phase transmission (blue dash-dotted line 2) and phase reflection (green dash-dotted line 3) coefficients. The power transmission spectrum is shown with the solid blue line 1 for comparison. Other parameters are the same as in Fig. 1.

The phase transmission spectrum is a continuous function and the phase reflection spectrum has unremovable offset at the points $\Psi_s = \pi k$. At the points (frequencies) of the maximal transmissivity (case of half-wave plate) the transmitted wave has the phase, which is multiple of π and the reflective wave changes phase by jumping on π . For the case of quarter-wave plate (minimum transmissivity and maximum reflectivity), the phase of the transmitted wave has values multiple of odd numbers of $\pi/2$ and the phase of the reflection wave is multiple of odd numbers of π .

The both unwrapped phase spectra experience a visible modulation that is the result of the effect of Fabry–Perot fringes. This modulation leads to well-pronounced oscillation behavior with period of π in the derivative of the phase, $d\varphi_{t,r}^{umw}(\Psi_s)/d\Psi_s$ (see Fig. 2b). As follows from Eqs (7) and (8), both derivatives can be calculated as:

$$\begin{aligned} \frac{d\varphi_t^{umw}(\Psi_s)}{d\Psi_s} &= -\sqrt{\frac{\varepsilon_0}{\varepsilon_s}} + \frac{d \arctan(\alpha^+ \tan(\Psi_s))}{d\Psi_s} = \\ &= -\sqrt{\frac{\varepsilon_0}{\varepsilon_s}} + \frac{\alpha^+}{\cos^2(\Psi_s) + (\alpha^+)^2 \sin^2(\Psi_s)} = \\ &= -\sqrt{\frac{\varepsilon_0}{\varepsilon_s}} + \alpha^+ T(\Psi_s), \quad \frac{d\varphi_r^{umw}(\Psi_s)}{d\Psi_s} = \alpha^+ T(\Psi_s). \end{aligned} \quad (11)$$

As seen, the derivative of the phase coefficients with respect to Ψ_s is proportional to power transmission coefficient with proportionality factor α^+ . We can conclude that extremal points of $d\varphi_{t,r}^{umw}(\Psi_s)/d\Psi_s$ and $T(\Psi_s)$ coincide. It means that phase coefficients have inflection points at the extremal points of the power coefficients.

Thus, we showed that the phenomenon of the Fabry–Perot fringes for dielectric plate can be easily traced in the phase spectra as the emergence of the inflection points. These points correspond to extrema in power spectra. Moreover, first derivative of the phase spectrum coincides up to a prefactor with the power transmission coefficient. This prefactor is a combination of the dielectric permittivities of the substrate and the ambient medium.

2.2. A thin conductive layer over interface

Another useful example is a thin conductive layer. The latter is formed by strongly localized mobile carriers. It is a key component of modern plasmonic devices. For example, doped semiconductor QW heterostructures or monoatomic layers of graphene provide nanometer scaled electron localization in one dimension. For interaction with relatively large wavelength of radiation this electron gas can be treated as delta-thin conductive layer.

In sub- and THz frequency ranges, the high-frequency response of the conductive layer is well described by Drude–Lorentz model. In the framework of this model, the frequency dispersion of the electron conductivity is read as

$$\sigma^{2D}(\omega) = \frac{e^2 n_{2D}}{m^*} \frac{i}{\omega + i\gamma_e}, \quad (12)$$

where n_{2D} and m^* are the electron concentration and the effective mass, respectively. Parameter γ_e describes electron scattering and is determined by particular electron collision mechanisms. The complex-valued transmission and reflection coefficients for the model of the conductive layer placed between two dielectric half-spaces with permittivities ε_1 and ε_2 have the following forms:

$$t(\omega) = t_0 \frac{\omega + i\gamma_e}{\omega + i(\Gamma_e + \gamma_e)}, \quad r(\omega) = \frac{-i\Gamma_e + r_0(\omega + i\gamma_e)}{\omega + i(\Gamma_e + \gamma_e)}, \quad (13)$$

where $\Gamma_e = 2\pi e^2 n_{2D} / m^* c \sqrt{\varepsilon_{eff}}$ with

$$\sqrt{\varepsilon_{eff}} = (\sqrt{\varepsilon_1} + \sqrt{\varepsilon_2})/2. \text{ In literature, parameters } \Gamma_e \text{ and } \gamma_e$$

are often mentioned as rates of radiative and non-radiative losses, respectively [36]. Two factors,

$$t_0 = 2\sqrt{\varepsilon_1} / (\sqrt{\varepsilon_1} + \sqrt{\varepsilon_2}) \text{ and } r_0 = (\sqrt{\varepsilon_1} - \sqrt{\varepsilon_2}) / (\sqrt{\varepsilon_1} + \sqrt{\varepsilon_2}),$$

are the standard Fresnel's amplitude transmission and reflection coefficients of the interface without the conductive layer. The power transmission, $T(\omega) = \sqrt{\varepsilon_2/\varepsilon_1} |t(\omega)|^2$, reflection, $R(\omega) = |r(\omega)|^2$, and absorption, $A(\omega) = 1 - T(\omega) - R(\omega)$, coefficients take the form:

$$\begin{aligned} T(\omega) &= T_0 \frac{\omega^2 + \gamma_e^2}{\omega^2 + (\Gamma_e + \gamma_e)^2}, \\ R(\omega) &= \frac{\omega^2 R_0 + (\Gamma_e \pm |r_0| \gamma_e)^2}{\omega^2 + (\Gamma_e + \gamma_e)^2}, \\ A(\omega) &= \frac{2\Gamma_e \gamma_e (1 \mp |r_0|)}{\omega^2 + (\Gamma_e + \gamma_e)^2}. \end{aligned} \quad (14)$$

Here, $T_0 = \sqrt{\varepsilon_2/\varepsilon_1} t_0^2$ and $R_0 = r_0^2$ are standard transmissivity and reflectivity of the interface in the absence of the conductive layer. Note that $T_0 + R_0 = 1$. Upper (lower) signs correspond to a negative (positive) r_0 . Negative r_0 corresponds to the case (I) when *em* wave travelling in an optically low dense medium strikes the surface of an optically denser medium ($\varepsilon_1 < \varepsilon_2$). Positive r_0 corresponds to the opposite case (II). As seen, $T(\omega)$, $R(\omega)$ as well as $A(\omega)$ are monotonic functions of frequency. At the low frequencies, such as $\omega \ll \Gamma_e, \gamma_e$,

$$T(\omega) \rightarrow T_0 \gamma_e^2 / (\Gamma_e + \gamma_e)^2 < T_0,$$

$$R(\omega) \rightarrow (\Gamma_e \pm |r_0| \gamma_e)^2 / (\Gamma_e + \gamma_e)^2, \text{ and}$$

$A(\omega) = 2\Gamma_e \gamma_e (1 \mp |r_0|) / (\Gamma_e + \gamma_e)^2$. For the case (I), the reflectivity is larger and the absorptivity is smaller than for the case (II). The transmissivity is the same for both cases. At high frequencies, such as $\omega \gg \Gamma_e, \gamma_e$, the response of the conductive layer becomes negligibly small and $T(\omega) \rightarrow T_0$, $R(\omega) \rightarrow R_0$ and $A(\omega) \rightarrow 0$.

Modifications of phase of the wave under transmission and reflection (the phase coefficients) can exhibit more interesting behavior. From Eqs (13) and definition (2), we obtain that

$$\varphi_t(\omega) = -\arctan\left(\frac{\omega\Gamma_e}{\omega^2 + \gamma_e(\Gamma_e + \gamma_e)}\right). \quad (15)$$

Analytical expression of the phase reflection coefficient is different for the cases (I) and (II). In the case (I):

$$\varphi_r(\omega) = -\pi + \arctan\left(\frac{\omega\Gamma_e(1 - |r_0|)}{|r_0|\omega^2 + (\Gamma_e + \gamma_e)(\Gamma_e + |r_0|\gamma_e)}\right). \quad (16)$$

In the case (II): if denominator $|r_0|\omega^2 + (\Gamma_e + \gamma_e)(|r_0|\gamma_e - \Gamma_e) > 0$, then

$$\varphi_r(\omega) = -\arctan\left(\frac{\omega\Gamma_e(1 + |r_0|)}{|r_0|\omega^2 + (\Gamma_e + \gamma_e)(|r_0|\gamma_e - \Gamma_e)}\right), \quad (17)$$

otherwise

$$\varphi_r(\omega) = -\pi - \arctan\left(\frac{\omega\Gamma_e(1 + |r_0|)}{|r_0|\omega^2 + (\Gamma_e + \gamma_e)(|r_0|\gamma_e - \Gamma_e)}\right). \quad (18)$$

In contrast to the power coefficients, the phase ones exhibit non-monotonic behavior with at least one extremal point. Indeed, in the case (I), $\varphi_t \rightarrow 0$, $\varphi_r \rightarrow -\pi$ for both limits of $\omega \rightarrow 0$ and ∞ . For the case (II), φ_t remains the same as for the case (I) and asymptotic behavior of φ_r depends on the ratio, $|r_0| \gamma_e \Gamma_e$. If $|r_0| \gamma_e \Gamma_e > 1$, then $\varphi_r \rightarrow 0$ at $\omega \rightarrow 0$, otherwise $\varphi_r \rightarrow -\pi$; at $\omega \rightarrow \infty$, $\varphi_r \rightarrow 0$ and it does not depend on ratio of $|r_0| \gamma_e \Gamma_e$. Thus, for case (I) both $\varphi_t(\omega)$ and $\varphi_r(\omega)$ have non-monotonic behavior. Also, non-monotonic behavior of $\varphi_r(\omega)$ is realized in the case (II), if $|r_0| \gamma_e \Gamma_e > 1$.

If the conductive layer is placed into uniform dielectric media, ($\varepsilon_1 = \varepsilon_2 = \varepsilon$) $\varepsilon_{eff} = \varepsilon$, $t_0 = 1$, $r_0 = 1$, then formulas for the power and phase coefficients are essentially simplified:

$$\begin{aligned} T(\omega) &= \frac{\omega^2 + \gamma_e^2}{\omega^2 + (\Gamma_e + \gamma_e)^2}, \\ R(\omega) &= \frac{\Gamma_e^2}{\omega^2 + (\Gamma_e + \gamma_e)^2}, \\ A(\omega) &= \frac{2\Gamma_e \gamma_e}{\omega^2 + (\Gamma_e + \gamma_e)^2}. \end{aligned} \quad (19)$$

$$\varphi_t(\omega) = -\arctan\left(\frac{\omega\Gamma_e}{\omega^2 + \gamma_e(\Gamma_e + \gamma_e)}\right), \quad (20)$$

$$\varphi_r(\omega) = -\pi + \arctan\left(\frac{\omega}{\Gamma_e + \gamma_e}\right).$$

Typical behavior of the power and phase coefficients are shown in Figs 3 for the case (I) and in Figs 4 for the case (II). In calculations, we set the following parameters of electrons $n_{2D} = 5 \cdot 10^{12} \text{ cm}^{-2}$, $m^* = 0.22m_e$ (m_e is free electron mass) and $\gamma_e = 0.8 \text{ THz}$. The latter corresponds to the electron mobility of $10^4 \text{ cm}^2/\text{V}\cdot\text{s}$. The selected values of the parameters correspond to the typical parameters of AlGaIn/GaN QW at liquid nitrogen temperatures. For three considered types of the interface with $[\varepsilon_1 = 1, \varepsilon_2 = 9.7]$, $[\varepsilon_1 = 1, \varepsilon_2 = 5]$, and $[\varepsilon_1 = \varepsilon_2 = 1]$ (free-standing conductive layer in vacuum) we have that $T_0 = 0.74, 0.85, 1, R_0 = 0.26, 0.15, 0$ ($|r_0| = 0.51, 0.38$), $\Gamma_e = 0.58, 0.75, 1.2 \text{ THz}$ and parameter $|r_0|\gamma_e\Gamma_e = 0.7, 0.4, 0$.

As seen, in the case (I) power coefficients are monotonic functions. Particularly, electrons essentially suppress the transmissivity (panel (a)) of the structure at the frequencies $\omega/\gamma_e < 4$. The smaller $T(\omega)$ occurs for uniform dielectric medium (blue curves) and can be less than 20%. The same tendency is observed in the reflectivity spectra (panel (b)). The larger difference between dielectric permittivities of the media formed interface leads to an increase of the reflectivity and decrease of the total absorption (panel (c)) of the structure. At the frequencies $\omega/\gamma_e = 10$ the response of the conductive layer becomes very weak. As a result, $T(\omega)$ and $R(\omega)$ are saturated and tend to the corresponding values of T_0 and R_0 . At this absorption tends to zero.

The phase spectra (dash-dotted lines) demonstrate a non-monotonic behavior with an emergence of the minimal/maximal points in the transmission/reflection. The both phases are negative with modulation of the order of 0.2π . The position of the extremal points, $\omega_{\min/\max}$, and corresponding values of the phases in these points, $\varphi_{t, \min/r, \max}$, can be found analytically. We obtain

$$\omega_{\min} = \sqrt{\gamma_e(\Gamma_e + \gamma_e)},$$

$$\varphi_{t, \min} = -\arctan\left(\frac{\Gamma_e}{2\sqrt{\gamma_e(\Gamma_e + \gamma_e)}}\right) = -\arctan\left(\frac{\Gamma_e}{2\omega_{\min}}\right) \quad (21)$$

and

$$\omega_{\max} = \sqrt{\frac{(\Gamma_e + \gamma_e)(\Gamma_e + |r_0|\gamma_e)}{|r_0|}},$$

$$\varphi_{r, \max} = -\pi + \arctan\left(\frac{\Gamma_e(1 - |r_0|)}{2|r_0|\omega_{\max}}\right). \quad (22)$$

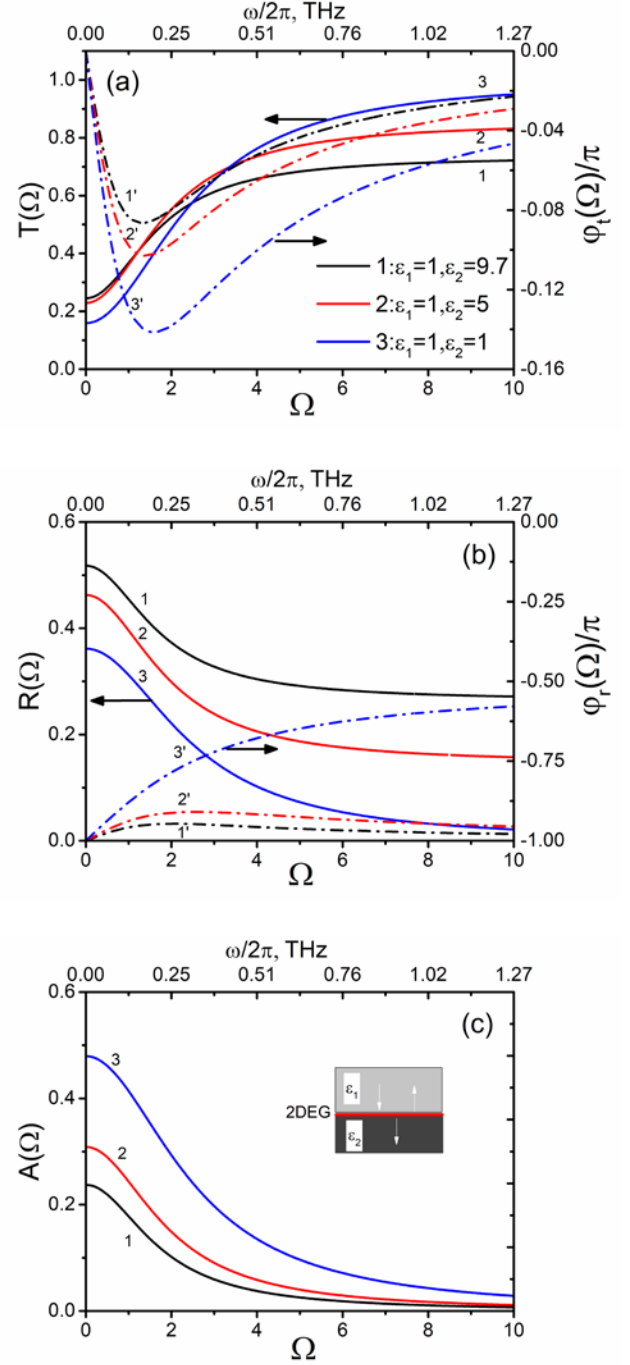


Fig. 3. The transmission (a), reflection (b) and absorption (c) spectra as functions of dimensionless frequency, $\Omega = \omega/\gamma_e$ of the conductive layer lying on three different interfaces corresponding to the case I. The solid lines 1–3 are power coefficients and the dash-dotted lines 1'–3' are phase coefficients. The upper axis is rescaled according to the parameters of conductive layer listed in the text.

Note, the latter is valid if $r_0 \neq 0$. For the conductive layer in the uniform media, $r_0 = 0$, phase reflection coefficient is the monotonic function defined by the second equation (20)). The decrease of Γ_e with an increase of the effective dielectric permittivity, ε_{eff} , is

a result of the red-shift of ω_{\min} and decreasing of $\varphi_{r, \min}$ for interface with optically denser medium. For three considered interfaces with $\varepsilon_2 = 9.7, 5, 1$, Eqs (21) give $\omega_{\min}/\gamma_e = 1.31, 1.4, 1.58$ (0.166, 0.177, 0.2 THz) and $\varphi_{r, \min} = -0.086\pi, -0.1\pi, -0.14\pi$, respectively. At the same time, for the first two interfaces $\omega_{\max}/\gamma_e = 2.05, 2.58$ (0.26, 0.33 THz) and $\varphi_{r, \max} = -0.946\pi, -0.91\pi$.

In the case (II), the transmissivity remains the same as in the case (I). However, the reflectivity (Fig. 4a) demonstrates inverse behavior in the low-frequency range, *i.e.*, the optically denser interface essentially suppresses reflection. It leads to an increase of total absorption (Fig. 4b) as compared with the case (I). At selected parameters, the phase reflection spectra are monotonic functions.

To finalize this section, it is worth to note that the phase transmission spectrum has minimum point. The coordinates of this point are described by the rates of radiative and non-radiative losses (see Eqs. (21)). Determination of this point in the measured spectra can be used for identification parameters of the conductive layer. Particularly,

$$\Gamma_e = -2\omega_{\min} \tan(\varphi_{t, \min}), \quad \gamma_e = \sqrt{\frac{\Gamma_e^2}{4} + \omega_{\min}^2} - \frac{\Gamma_e}{2}. \quad (23)$$

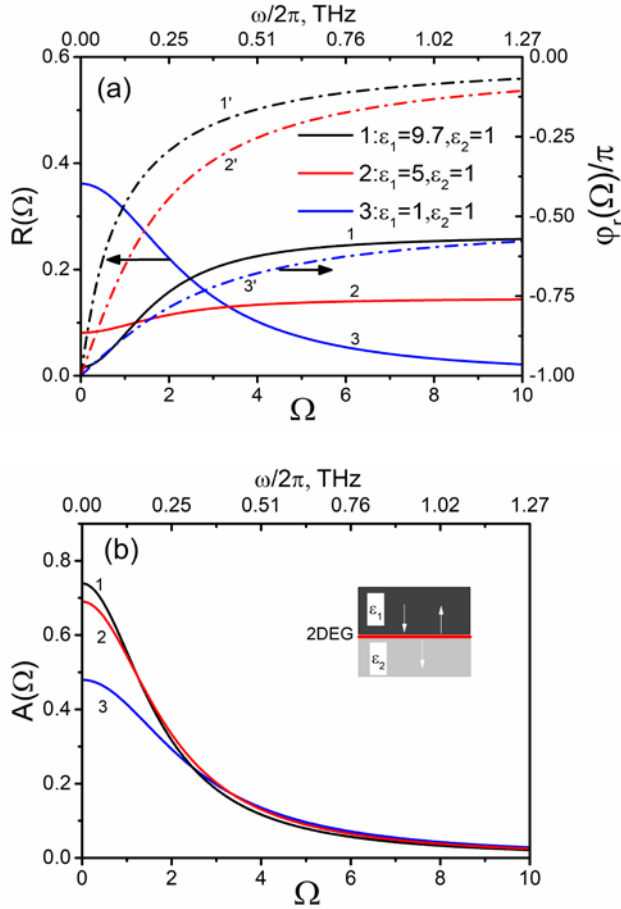


Fig. 4. The same as in Figs 3b and 3c for the case (II).

These parameters allow us to determine the electron concentration, n_{2D} and the electron mobility, μ_e :

$$n_{2D} = \frac{\Gamma_e m^* c \sqrt{\varepsilon_{eff}}}{2\pi e^2}, \quad \mu_e = \frac{e}{\gamma_e m^*}. \quad (24)$$

2.3. The conductive layer on a substrate

This model structure has a geometry close to that of the existing heterostructure samples. The complex-valued transmission and reflection coefficients of this structure can be written as follows:

$$t(\omega) = t_s(\omega) \frac{\omega + i\gamma_e}{\omega + i\gamma_e + i\Gamma_e(1 + r_s(\omega))}, \quad (25)$$

$$r(\omega) = \frac{r_s(\omega)(\omega + i\gamma_e) - i\Gamma_e(1 + r_s(\omega))}{\omega + i\gamma_e + i\Gamma_e(1 + r_s(\omega))}, \quad (26)$$

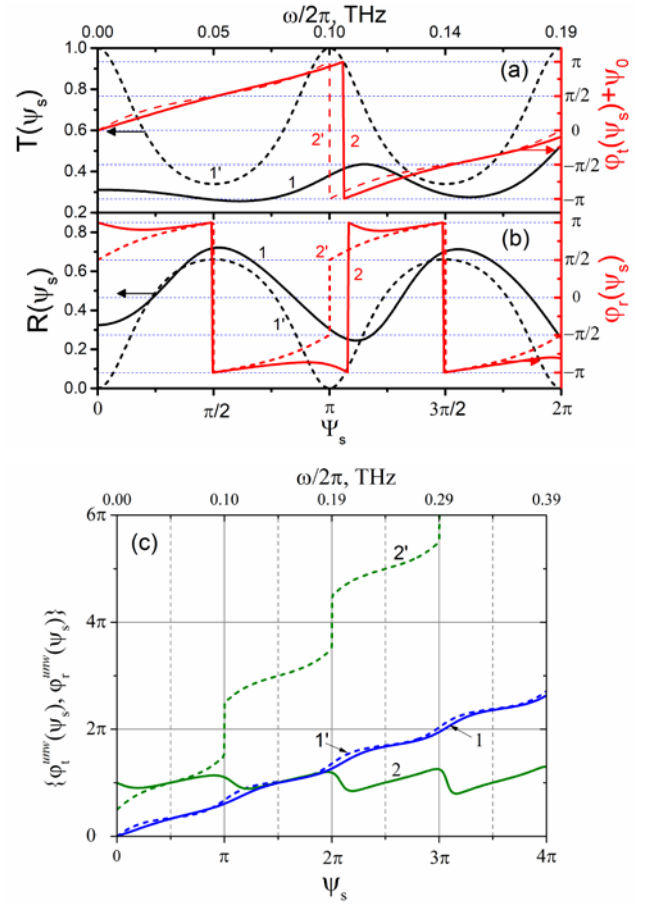


Fig. 5. Power (black lines $1, 1'$) and phase (red lines $2, 2'$) transmission (panel (a)) and reflection (panel (b)) coefficients as functions of Ψ_s . Panel (c): the phase transmission (blue lines $1, 1'$) and phase reflection (green lines $2, 2'$) coefficients in the representation of the unwrapped phase. In all the panels, solid lines correspond to the structure *2D conductive layer on substrate* and dashed lines correspond to the single substrate. The parameters of substrate are the same as in Fig. 1. The conductive layer is described by the following parameters: the electron 2D-concentration is equal to $3 \cdot 10^{12} \text{ cm}^{-2}$ ($\Gamma_e = 0.72 \text{ THz}$ at the effective mass of $0.22m_e$ and $\varepsilon_0 = 1$) and $\gamma_e = 1 \text{ THz}$.

where $t_s(\omega)$ and $r_s(\omega)$ are the complex-valued transmission and reflection coefficients of the substrate (see Eqs (4) and (5)), respectively. Also, we assumed the Drude–Lorentz dispersion of the conductive layer given by Eq. (12), and the factor of radiative losses is expressed here as follows, $\Gamma_e = 2\pi e^2 n_{2D} / m^* c \sqrt{\varepsilon_0}$.

Figs 5 provide comparison between spectral characteristics of the structure *the conductive layer on a substrate* and a single dielectric plate. As seen, the presence of moderate values of electron concentration ($n_{2D} = 3 \cdot 10^{12} \text{ cm}^{-2}$) essentially modifies the power transmission and phase reflection spectra. The power reflection and phase transmission spectra are less sensitive to the presence of the conductive layer. Particularly, the effect of the electrons manifests itself as well-pronounced suppression of *em* wave transmission in the low-frequency range, $\omega/\gamma_e \leq 1$. The power transmission and reflection spectra become non-periodic functions, while maximal/minimal values of $T(\omega)/R(\omega)$ -dependences are blue-shifted with respect to characteristic frequencies $\Psi_s = \pi k$ (see solid lines in panels (a) and (b)). Also, the maximum of $T(\omega)$ and minimum of $R(\omega)$ do not reach values of 1 and 0, respectively. All of these is the result of essential Drude absorption of *em* wave by the conductive layer.

Additionally, it should be noted the modification of the offset by π that is realized in the phase reflection spectrum, for single substrate at the points $\Psi_s = \pi k$. Due to the presence of the conductive layer, $\varphi_r(\omega)$ acquires offset by 2π at the points corresponding to the minima of $R(\omega)$. As a result, the phase reflection spectrum in the representation of the unwrapped phase becomes a continuous function (see panel (c)).

3. Grating-based resonant plasmonic structures

As mentioned in Introduction, the plasmonic structures consisting of the conductive layer placed in the vicinity of the metallic grating are in the focus of the many modern THz applications. These plasmonic structures possess resonant properties due to the excitations of the 2D plasmons. The analysis of the resonant line in both amplitude and phase spectra can provide valuable information about parameters of the conductive layer. Particularly, we will show here that characteristic parameters of the radiative, Γ_e , and non-radiative, γ_e , losses can be directly obtained from the phase transmission spectrum.

The simplified analytic theory of the interaction of *em* wave with such structures was developed by S. Mikhailov in [36]. Following his approach, the complex transmission coefficient for the structure with “perfect metallic grating-conductive layer” in the frequency region of the *m*-th order plasmon resonance can be written as follows:

$$t(\omega) = \frac{\omega^2 - \omega_{0,m}^2 + i\gamma_e \omega}{\omega^2 - \omega_{0,m}^2 + i\omega(\tilde{\Gamma}_{e,m} + \gamma_e)}, \quad (27)$$

where resonant frequency $\omega_{0,m} = \omega_{p,m} \chi_0(m, f, d)$ is the renormalized frequency of the *ungated* 2D plasmons, $\omega_{p,m} = \sqrt{2\pi e^2 n_0 |q_m| / m^* \varepsilon}$, calculated at characteristic grating wavevector, $q_m = 2\pi m / a_g$ (a_g – grating period). The parameter $\tilde{\Gamma}_{e,m} = \Gamma_e \chi_1(m, f, d)$ characterizes renormalized radiative decay. The renormalization functions $\chi_{0,1}(m, f, d)$ contain geometrical parameters of the structure: grating filling factor, f , distance between grating and the conductive layer and also depend on the order of plasmon resonance (for details see [36]).

It should be noted that approximate expression (27) is obtained under a few assumptions. Among the others, it is assumed: (I) the delta-thin perfect metallic grating with semi-elliptic profile of the conductive strip, (II) high quality plasmon resonances ($\omega_{0,m} \gg \tilde{\Gamma}_{e,m}, \gamma_e$) and (III) negligibly small interaction between neighboring resonances. Nevertheless, Eq. (27) provides rather sufficient description of the resonant line in both power and phase spectra (see below comparison between Michailov’s approach and rigorous electrodynamic simulation).

Eq. (27) gives that

$$T(\omega) = 1 - \frac{\omega^2 (\tilde{\Gamma}_{e,m}^2 + 2\tilde{\Gamma}_{e,m} \gamma_e)}{(\omega^2 - \omega_{0,m}^2)^2 + \omega^2 (\tilde{\Gamma}_{e,m} + \gamma_e)^2}, \quad (28)$$

$$\varphi_t(\omega) = \arctan \left(\frac{(\omega_{0,m}^2 - \omega^2) \omega \tilde{\Gamma}_{e,m}}{(\omega^2 - \omega_{0,m}^2)^2 + \gamma_e (\tilde{\Gamma}_{e,m} + \gamma_e) \omega^2} \right). \quad (29)$$

Far away from resonant frequencies ($\omega \gg \omega_{0,m}$), the power transmission coefficient (28) is close to unity. It corresponds to weak Drude–Lorentz response of the conductive layer and weak interaction of the perfect metallic grating with *em* wave. In the vicinity of the resonant frequency $T(\omega)$ provides Lorentz-type shape of the spectral line with resonant values, $T_{res,m} \equiv T(\omega_{0,m})$ and full-width at half-minimum (FWHM), $\delta_{t,m}$. Both characteristics are:

$$T_{res,m} = \gamma_e^2 / (\tilde{\Gamma}_{e,m} + \gamma_e)^2, \quad \delta_{t,m} = \tilde{\Gamma}_{e,m} + \gamma_e. \quad (30)$$

Two mentioned characteristics of the resonant line in the power spectrum can be used for determination of non-radiative and radiative decay rates. They are:

$$\gamma_e = \sqrt{T_{res,m}} \delta_{t,m}, \quad \tilde{\Gamma}_{e,m} = \delta_{t,m} (1 - \sqrt{T_{res,m}}). \quad (31)$$

The obtained form of the phase transmission spectra (29) corresponds to the definition (3), at $x > 0$ ($\text{Re}[t(\omega)]$ is always positive). As seen, $\varphi_t(\omega)$ exhibits

non-monotonic alternating behavior, $\varphi_t(\omega) > 0$, if $\omega > \omega_{0,m}$ and $\varphi_t(\omega) < 0$, if otherwise. Zero of the phase transmission coefficient corresponds to the minimum in the power transmission coefficient. This fact is the result of the Bode relations [45]. Far away from resonant frequencies, we obtain $\varphi_t(\omega) \rightarrow 0$. Such behavior denotes that $\varphi_t(\omega)$ has at least two extrema. Their positions and values can be found from the equation $dg(\omega)/d\omega = 0$, where $g(\omega)$ is the argument of arctangent in Eq. (29). For simplicity, we introduce variable $\theta = (\omega_{0,m}^2 - \omega^2)/\omega$. Then, $dg(\omega)/d\omega = dg(\theta)/d\theta \times d\theta/d\omega$ (note, $d\theta/d\omega = -(\omega_{0,m}^2 + \omega^2)/\omega$ is always negative) and the search of characteristic frequencies of these extrema is reduced to the solution of equation

$$\frac{dg(\theta)}{d\theta} \equiv \frac{d}{d\theta} \left[\frac{\Gamma_{e,m}\theta}{\theta^2 + \gamma_e(\tilde{\Gamma}_{e,m} + \gamma_e)} \right] = 0. \quad (32)$$

The latter gives two roots

$$\theta_{1,2} = \pm \sqrt{\gamma_e(\tilde{\Gamma}_{e,m} + \gamma_e)}, \quad (33)$$

which correspond to

$$\omega_{1,2} = \sqrt{\omega_{0,m}^2 + \frac{\gamma_e(\tilde{\Gamma}_{e,m} + \gamma_e)}{4}} \pm \frac{\sqrt{\gamma_e(\tilde{\Gamma}_{e,m} + \gamma_e)}}{2}. \quad (34)$$

The distance between positions of these extrema, $\Delta\omega_{res} = |\omega_2 - \omega_1|$, and swing of the phase modulation, $\Delta\varphi_{t,res} = |\varphi_t(\omega_2) - \varphi_t(\omega_1)|$, are:

$$\Delta\omega_{res} = \sqrt{\gamma_e(\tilde{\Gamma}_{e,m} + \gamma_e)}, \quad (35)$$

$$\varphi_{t,res} = 2 \arctan \left(\frac{\tilde{\Gamma}_{e,m}}{2\sqrt{\gamma_e(\tilde{\Gamma}_{e,m} + \gamma_e)}} \right).$$

Using two resonant characteristics $\Delta\omega_{res}$ and $\Delta\varphi_{t,res}$, we can alternatively determine $\tilde{\Gamma}_{e,m}$ and γ_e from resonant peculiarities in the phase transmission spectrum:

$$\tilde{\Gamma}_{e,m} = 2\Delta\omega_{res} \tan \frac{\Delta\varphi_{t,res}}{2}, \quad (36)$$

$$\gamma_e = \sqrt{\frac{\tilde{\Gamma}_{e,m}^2}{4} + \Delta\omega_{res}^2} - \frac{\tilde{\Gamma}_{e,m}}{2}.$$

Examples of the power and phase transmission spectra for the particular case of the modeled plasmonic structure are shown in Fig. 6. The sketch of the considered structure is shown in the inset. We considered the delta-thin gold grating with the semi-elliptical profile of conductive strip, $\sigma_g(x) = 2 \times 10^{12} \sqrt{1 - (2x/w_g)^2}$ cm/s.

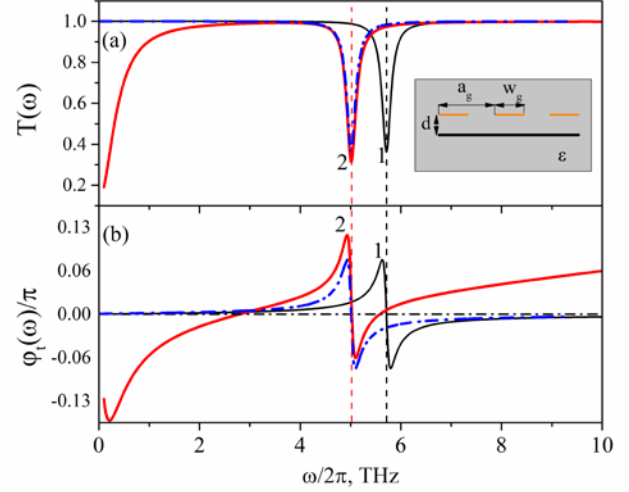


Fig. 6. Power (a) and phase (b) transmission spectra obtained in accord with Eqs (28) and (29) containing the parameters listed in the text (black lines 1) and full electrodynamic calculation (red lines 2). The dash-dotted blue lines are the same black lines but centered with respect to resonant frequency 5 THz realized for the red curves. (Color online)

The grating period, a_g , strip width, w_g , are assumed to be equal to 1 and 0.5 μm (grating filling factor $f = 0.5$), respectively. The conductive layer located at the distance, $d = 0.025 \mu\text{m}$, from the grating. We set the following parameters for the conductive layer: electron effective mass $m^* = 0.22m_e$ (m_e is the free electron mass), sheet electron concentration $n_e = 6 \cdot 10^{12} \text{ cm}^{-2}$, and mobility $\mu_e = 10^4 \text{ cm}^2/\text{V}\cdot\text{s}$. The selected parameters are close to those realized in the high-quality AlGaIn/GaN QW heterostructures. Whole structure is placed into the uniform media with $\epsilon = 1$.

For these parameters, $\omega_{p,1} = 2\pi \times 8.3 \text{ THz}$, $\Gamma_e = 1.44 \text{ THz}$ and $\gamma_e = 0.8 \text{ THz}$. The geometrical factors: $\chi_0 = 0.68$ and $\chi_1 = 0.36$. As a result, the resonant frequency $\omega_{0,1} = 2\pi \times 5.7 \text{ THz}$ and renormalized radiative decay rate $\tilde{\Gamma}_{e,1} = 0.53 \text{ THz}$. The resulting power and phase transmission spectra obtained in the frames of Michailov's approach demonstrate the existence of the high-quality plasmon resonance for which $\omega_{0,1}/\{\gamma_e, \tilde{\Gamma}_{e,1}\} = \{45, 68\} \gg 1$. Here, we restrict ourselves by the analysis of the 1-st order plasmon resonances ($m = 1$). For comparison, we performed complete electrodynamic simulation of power and phase spectra (see red curves 2) in the framework of integral equations method [34, 46]. The exact calculations give slightly smaller resonant frequency, $\omega_{0,1} = 2\pi \times 5 \text{ THz}$. The origin of this deviation was discussed in Ref. [47]. However, the obtained form of the resonant lines in the power and phase spectra can be well-described by the approximate formulas (28) and (29) with the resonant frequency obtained from exact calculations (see dash-dotted blue lines).

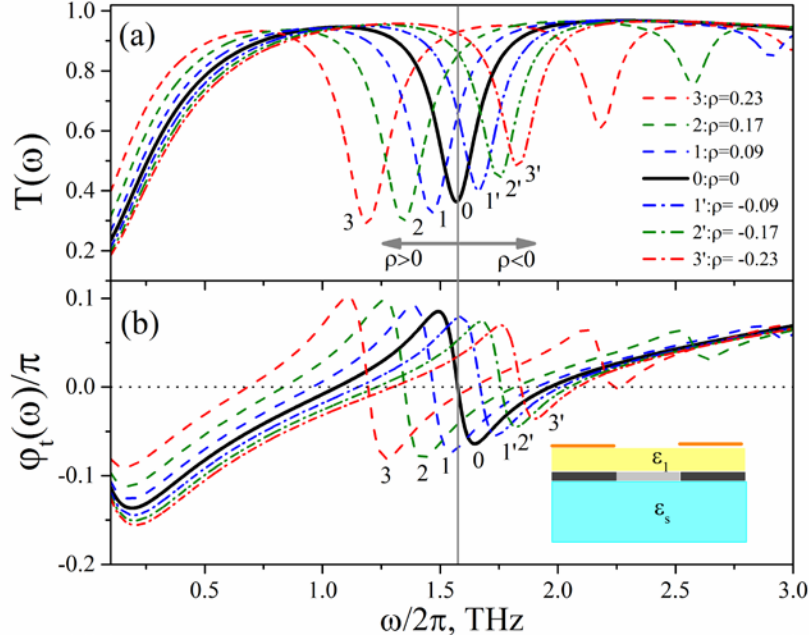


Fig. 7. Power (a) and phase (b) transmission coefficients calculated at several values of the modulation degree for the conductive layer concentration, ρ , in the plasmonic structure with membrane-like substrate ($D_s = 1 \mu\text{m}$). The electron concentration in the ungated region of the conductive layer, $n_{0,\text{un}} = 5 \cdot 10^{12} \text{ cm}^{-2}$, is assumed to be constant. The dielectric permittivities of the barrier layer, ϵ_1 , and substrate, ϵ_s , are equal to 9 and 9.72, respectively. The thickness of barrier layer is equal to $0.025 \mu\text{m}$. The gold grating has a step-like profile with the period close to $1 \mu\text{m}$ and filling factor 0.5. (Color online)

Now, we check that resonant peculiarities of phase transmission spectra can be used for inverse electrodynamic problem, *i.e.*, extraction of the parameters of the conductive layer. From the phase spectrum (red curve 2 in Fig. 6b), we have that $\Delta\phi_{t,\text{res}} = 0.56$ and $\Delta\omega_{\text{res}} = 2\pi \times 0.17 \text{ THz}$. The formulas (36) give that $\tilde{\Gamma}_{e,m} = 0.62$ and $\gamma_e = 0.81$. The first parameter is used to estimate the value of the conductive layer electron concentration, $n_e = c \sqrt{\epsilon} m^* \tilde{\Gamma}_{e,m} / 2\pi e^2 \chi_1$. The second parameter directly provides the value of the electron mobility inherent to the conductive layer, $\mu_e = e/m^* \gamma_e$. The obtained values $n_e = 7.1 \cdot 10^{12} \text{ cm}^{-2}$ and $\mu_e = 9840 \text{ cm}^2/\text{V}\cdot\text{s}$ are close to the input parameters $n_e = 6 \cdot 10^{12} \text{ cm}^{-2}$ and $\mu_e = 10^4 \text{ cm}^2/\text{V}\cdot\text{s}$.

Thus, definite peculiarities of resonant line in phase transmission spectra can be used for basic characterization of the conductive layer, particularly, for determination of electron concentration and mobility.

4. Electrical control of the phase and power transmission spectra

As it was shown in the previous section, the resonant peculiarities in the power and phase spectra are directly related to the excitation of 2D plasmons under the grating. The spectral position and form of resonant lines depend on several parameters [33, 48], namely: period of the grating, grating filling factor, dielectric ambience of

the conductive layer and, what is important, the electron concentration. The latter provides perspective method of fast electrical control of the optical characteristics of the plasmonic structures. Indeed, the hybrid plasmonic structure with the conductive layer can be configured as a grating-gate field-effect transistor (FET), where the plasmon spectra and plasmon resonances can be modified by an applied gate-to-channel voltage due to a spatial modulation of the electron concentration. Such possibility was experimentally verified in Refs. [26, 49], a theoretical approach for description of the plasmonic structure with non-uniform profile of the electron concentration was proposed in Ref. [46].

However, the mentioned papers were focused on the study of amplitude characteristics. Here, we discuss the possibility to control the phase characteristics. The results shown in Figs 7 to 10 are obtained numerically by using the method for solving the Maxwell equations from Ref. [46], which was generalized by us for the multi-layered geometry of the structure. Particularly, we considered two types of AlGaIn/GaN plasmonic structure on membrane-like and thick SiC substrates. The selected parameters of the plasmonic structures are similar to those of the existing structures [28, 29].

We assume that applied grating strips-to-channel voltage can modify electron concentration of the conductive layer under the grating strip (gate region). In the biased structure, the electron concentration in the conductive layer inherent to the gated region, $n_{0,g}$, can be smaller/larger (depending on the sign of the applied bias)

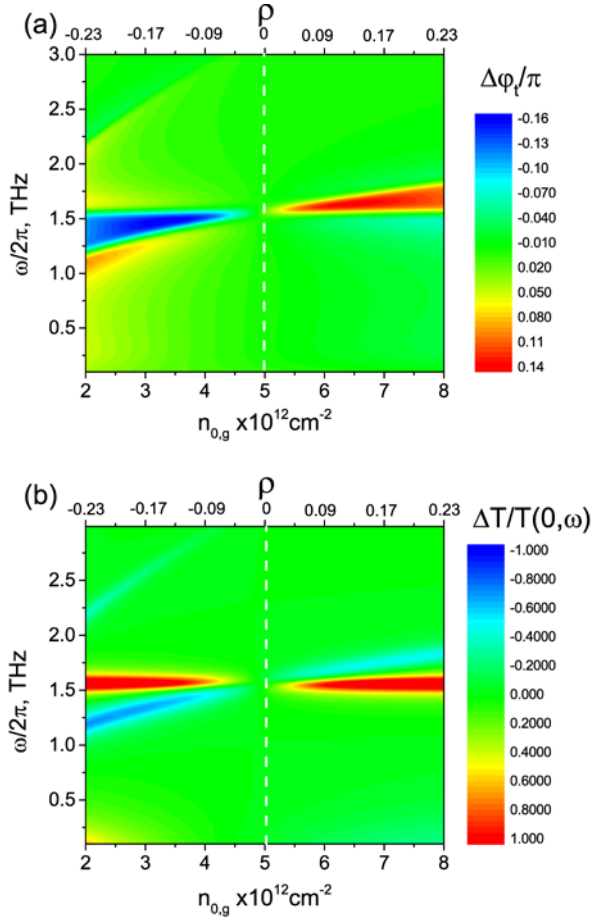


Fig. 8. Contour plots in the plane $\{n_{0,g}, \omega\}$ of the phase difference (a) and relative transmittivity (b) of the plasmonic structure with the same parameters as in Fig. 7. (Color online)

than that under the grating opening (ungated region), $n_{0,ug}$. To characterize modulation of the profile typical for the electron concentration, we introduced the following parameter: $\rho = (n_{0,g} - n_{0,ug}) / (n_{0,g} + n_{0,ug})$. At $\rho > 0$, an additional electrical doping of gated region occurs. Otherwise, an electrical depletion is realized. The profile of the electron concentration is assumed to be a step-like.

The spectra of the power and phase transmission coefficients for the plasmonic structure with thin substrate at particular values of ρ are depicted in Figs 7a and 7b, respectively. As seen, the negative/positive degree of the modulation induces a red/blue shift of the resonant line with respect to the unbiased structure ($\rho = 0$). Even the moderate value of modulation $\rho = \pm 0.23$ ($n_{0,g} - n_{0,ug} = \pm 3 \cdot 10^{12} \text{ cm}^{-2}$ at $n_{0,ug} = 5 \cdot 10^{12} \text{ cm}^{-2}$) provides a shift of the resonant frequency of 1.58 THz estimated as ± 0.23 THz. The intensity of plasmon resonance slightly increases at $\rho < 0$ and decreases at $\rho > 0$. For example, the swing of phase modulation near the resonant frequency at $\rho = 0$ is equal to 0.15π and reaches the values 0.18π at $\rho = -0.23$ and 0.1π at $\rho = 0.23$. In this case, the resonant values of transmittivity change from 0.29 (at 1.18 THz) to 0.48 (1.82 THz) at variation of ρ from -0.23 to 0.23 .

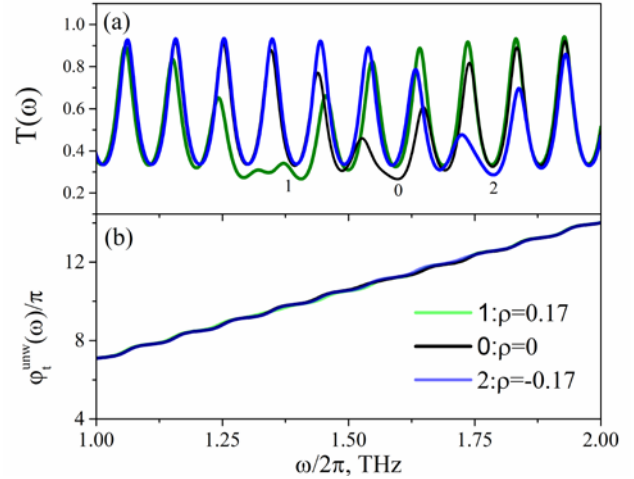


Fig. 9. The same as in Fig. 7 for the structure with the thick substrate ($D_s = 500 \mu\text{m}$).

For many THz applications, particularly in the field of THz holography, it is necessary to create a controllable phase shift between two coherent beams. For this purpose, it is possible to use the plasmonic structure, in which one part of the illuminated grating area is biased and another one is unbiased. The contour plot in Fig. 8a illustrates the phase difference, $\Delta\phi_t = \phi_t(\rho, \omega) - \phi_t(0, \omega)$, between phases of the beams transmitted through the biased and unbiased parts of the structure. As seen, there are two “islands” with $\Delta\phi_t < 0$ and $\Delta\phi_t > 0$. The first island is located in the lower frequency range 1.25 to 1.5 THz and second one is located in the higher frequency range 1.5...1.75 THz. Location of these “islands” corresponds to the total linewidth of the plasmon resonance of unbiased structure. It denotes us that the large modulation of the phase difference $\Delta\phi_t$ can be achieved within the frequency interval 1.25...1.75. Apparently, maximal modulation from -0.16π to 0.14π will be realized at the frequency of approximately 1.5 THz.

Together with phase modulation, the essential one with the amplitude of the transmitted waves is also possible. It is illustrated in Fig. 8b where we depicted the mapping of the relative transmittivity defined as $\Delta T/T(0, \omega) = (T(\rho, \omega) - T(0, \omega)) / T(0, \omega)$. Here, we also observed the existence of the several islands with essential values of modulation and different signs of this modulation. The red islands for which $\Delta T/T(0, \omega) > 0$ are located within the linewidth of plasmon resonance observed in the unbiased structure. The blue islands ($\Delta T/T_{ref} < 0$) are the traces that are followed by the motion of the resonant line under variation of ρ .

The spectra of the power and phase transmission coefficients for the plasmonic structure with thick substrate at particular values of ρ are depicted in Figs 9a and 9b, respectively. The effect of the substrate is crucial and leads to emergence of the Fabri–Perot fringes.

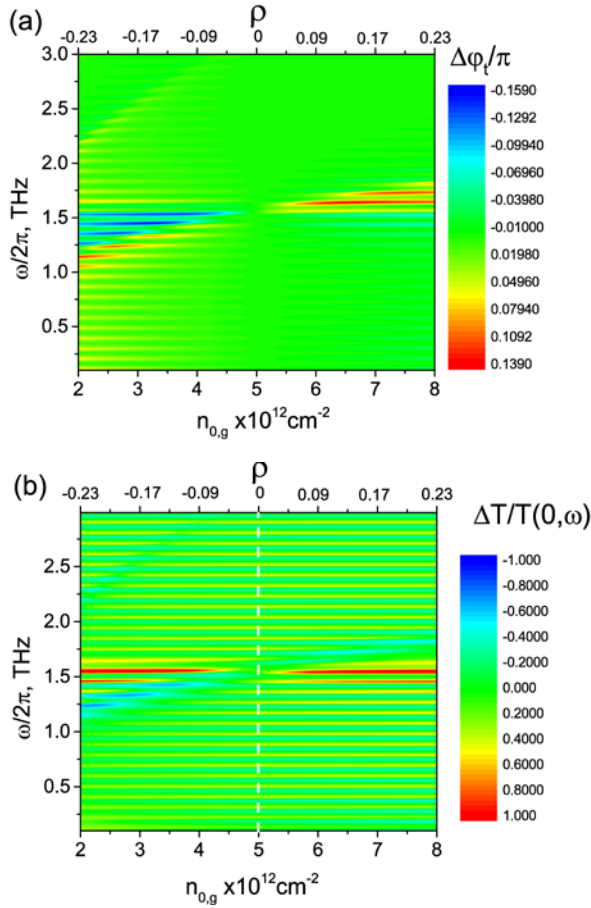


Fig. 10. The same as in Fig. 8 for the structure with the thick substrate ($D_s = 500 \mu\text{m}$). (Color online)

However, plasmon resonance in power spectra can be identified as an essential suppression of the Fabry–Perot oscillation in the particular frequency range. The phase spectra in the representation of the unwrapped phase are monotonic functions with the absence of visible signs of the plasmon resonance. It is the result of the large scaling of the unwrapped phase.

In this sense, the variable $\Delta\phi_i$ is more informative. The obtained form of the counter plot of this variable (see Fig. 10a) is similar to that shown in Fig. 8a for the structure with a thin substrate. However, characteristic islands of the essential modulations are experienced additional *incisions* due to the Fabry–Perot fringes. The same impact of the Fabry–Perot fringes is observed in the counter plot of the relative transmissivity $\Delta T/T(0, \omega)$ (see Fig. 10b).

We also can consider a possibility of phase modulation at constant amplitude. Indeed, a constant amplitude regime is the main operational mode of these phase modulators. According to Fig. 7, there are two almost antisymmetric wings of phase spectra at the vicinity of plasmonic resonance, which manifests itself as symmetric minimum on power transmission coefficient spectra. Thereafter we can choose two different levels of modulation with equal power transmission coefficients and different phase shifts.

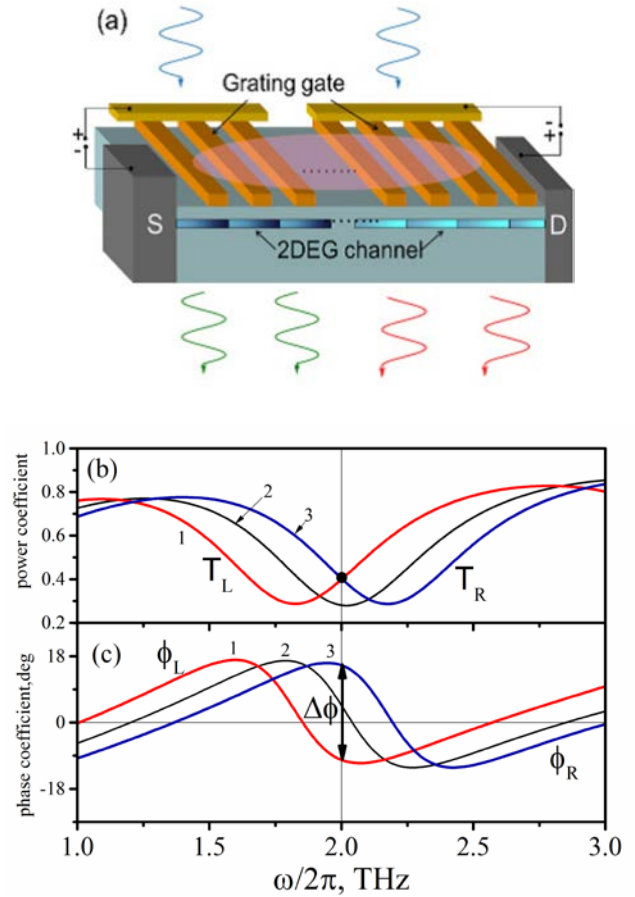


Fig. 11. (a) The schematic sketch of the proposed grating-based modulator. The power (b) and phase (c) transmission coefficients of the left (L) and right (R) parts of the device at different levels of modulation inherent to the conductive layer concentration. For the left part (1): $n_{0,ug} = 10^{13} \text{ cm}^{-2}$, $n_{0,g} = 8 \cdot 10^{12} \text{ cm}^{-2}$. For the right part (3): $n_{0,ug} = 10^{13} \text{ cm}^{-2}$, $n_{0,g} = 1.4 \cdot 10^{13} \text{ cm}^{-2}$. For the unmodulated channel (2): $n_0 = 10^{13} \text{ cm}^{-2}$. The electron mobility is assumed to be close to $3000 \text{ cm}^2/\text{V}\cdot\text{s}$ for both parts of device. The grating parameters are as follows: grating period is of $1 \mu\text{m}$, grating filling factor is of 0.7. The other parameters are the same as in Fig. 7.

Let us assume a particular plasmonic device (see Fig. 11a) that consists of two independent regions with different electrical gate-to-channel biases that induce two different modulation degree of electron gas. Say, the left part of the device is described by $\rho < 0$ and the right part by $\rho > 0$. The power and phase transmission spectra of these parts are shown in Figs 11b and 11c, respectively. As seen, there is the special frequency (2 THz), at which the amplitude spectra coincide, *i.e.*, beams propagating through left and right parts of the device have the same amplitudes, but they acquire the certain value of phase shift close to 24° (see panel (c)).

Thus, the performed analysis illustrates possibility to use the grating-gated plasmonic structures as a core element of electrically-controlled amplitude and phase modulators for THz frequency range.

5. Summary

We have analytically studied peculiarities of the amplitude (power) and phase transmission/reflection spectra of different thin-film semiconductor structures, including grating-based plasmonic structures with the thin layer of electrons, which can be considered as key components of modern THz devices. In particular, we have considered the non-resonant (optically thick dielectric substrate, the conductive layer between two dielectric media and electrons on dielectric substrate) and resonant (the conductive layer under subwavelength metallic grating) structures.

We have shown that extrema in the reflectance/transmittance spectra of the substrate, originated from Fabri–Perot modes, correspond to the particular offsets in the phase spectra. In the representation of the unwrapped phase, the phase transmission spectrum is a continuous function with inflection points corresponding to the extrema in power transmission. In this representation, the phase reflection spectrum has unremovable offsets by π at frequencies corresponding to the minima of the power reflection spectrum. We have ascertained that the first derivative of the phase spectra with respect to the frequency is in proportion to the power transmission spectra. For the structure *thin electron gas layer between dielectric media*, we found that the phase transmission spectrum is non-monotonic function with a minimum. Positions of this minimum depend on values of rates of radiative and non-radiative losses, which can be used for identification of basic parameters of the conductive layer (see Eq. (23)) from, for example, the appropriate THz-TDS measurements.

The structure *electron gas layer on dielectric substrate* reveals more complicated behavior of the power and phase spectra. In contrast to the single substrate, Drude absorption of *em* wave by electrons leads to aperiodic behavior of the power spectra in low-frequency range and essential modification of the phase reflection spectra. In the representation of the unwrapped phase, the phase reflection spectrum becomes continuous function without any offsets. At the same time, the phase transmission spectra of this structure and single substrate are weakly distinctive.

For the resonant plasmonic structure, namely, *the electron layer under a metallic grating*, we have shown that the form of the resonant line in the power transmission spectra can be approximately described by the Lorentz-like formula (see Eq. (28)). The values of transmission minimum and FWHM of resonant lines can be also used for determining the concentration and mobility of electrons in the conductive layer. Also, we found simple relations (see Eqs. (36)) between the characteristics of electrons and particular form of the phase transmission spectrum in the vicinity of the plasmon resonance.

Finally, we have demonstrated that grating-based plasmonic structure with particular spatial modulation of electron concentration in the conductive layer can be used as phase modulator for *em* waves in THz frequency range. The latter device can be used as THz-wavefront converters, multi-beam splitters with electrical control of operation parameters, including the spectral band.

We have suggested that these review and analysis can be useful for specialists working in the fields of THz physics and design of novel THz devices.

V.V.K. acknowledges the support from the Research Council of Lithuania (Lietuvos mokslo taryba) through the “T-HP” Project (Grant No. DOTSUT-184) funded by the European Regional Development Fund according to the supported activity “Research Projects Implemented by World-class Researcher Groups” under the Measure No. 01.2.2-LMT-K-718-03-0096.

References

1. Auston D.H., Cheung K.P., and Smith P.R. Picosecond photoconducting Hertzian dipoles. *Appl. Phys. Lett.* 1984. **45**, No 3. P. 284–286. <https://doi.org/10.1063/1.95174>.
2. Berry C.W. and Jarrahi M. Terahertz generation using plasmonic photoconductive gratings. *New J. Phys.* 2012. **14**. P. 105029. <https://doi.org/10.1088/1367-2630/14/10/105029>.
3. Castro-Camus E. and Alfaro M. Photoconductive devices for terahertz pulsed spectroscopy: a review [Invited]. *Photon. Res.* 2016. **4**, No 3. P. A36–A42. <https://doi.org/10.1364/PRJ.4.000A36>.
4. Apostolopoulos V. and Barnes M.E. THz emitters based on the photo-Dember effect. *J. Phys. D: Appl. Phys.* 2014. **47**. P. 374002. <https://doi.org/10.1088/0022-3727/47/37/374002>.
5. Sakai K. and Tani M. *Terahertz Optoelectronics (Topics in Applied Physics, vol. 97)*. Ed. K. Sakai. Berlin, Springer. 2005. P. 1–31.
6. Melentev G.A., Shalygin V.A., Vorobjev L.E. *et al.* Interaction of surface plasmon polaritons in heavily doped GaN microstructures with terahertz radiation. *J. Appl. Phys.* 2016. **119**. P. 093104. <https://doi.org/10.1063/1.4943063>.
7. Jakštas V., Grigelionis I., Janonis V. *et al.* Electrically driven terahertz radiation of 2DEG plasmons in AlGaIn/GaN structures at 110 K temperature. *Appl. Phys. Lett.* 2017. **110**. P. 202101. <https://doi.org/10.1063/1.4983286>.
8. Shalygin V.A., Moldavskaya M.D., Vinnichenko M.Y. *et al.* Selective terahertz emission due to electrically excited 2D plasmons in AlGaIn/GaN heterostructure. *J. Appl. Phys.* 2019. **126**. P. 183104. <https://doi.org/10.1063/1.5118771>.
9. Laurent T., Sharma R., Torres J. *et al.* Voltage-controlled sub-terahertz radiation transmission through GaN quantum well structure. *Appl. Phys. Lett.* 2011. **99**. P. 082101. <https://doi.org/10.1063/1.3627183>.

10. Persano A., Torres J., Koroteyev V.V. *et al.* On the transmission of terahertz radiation through silicon-based structures. *J. Appl. Phys.* 2014. **116**. P. 044504. <https://doi.org/10.1063/1.4890836>.
11. Rogalski A., Sizov F. Terahertz detectors and focal plane arrays. *Opto-Electron. Rev.* 2011. **19**, No 3. P. 346–404. <https://doi.org/10.2478/s11772-011-0033-3>.
12. Minkevicius L., Qi L., Siemion A. *et al.* Titanium-based microbolometers: Control of spatial profile of terahertz emission in weak power sources. *Appl. Sci.* 2020. **10**. P. 3400. <https://doi.org/10.3390/app10103400>.
13. Knap W., Dyakonov M., Coquillat D. *et al.* Field effect transistors for terahertz detection: Physics and first imaging applications. *J. Infrared Milli Terahz Waves.* 2009. **30**. P. 1319–1337. <https://doi.org/10.1007/s10762-009-9564-9>.
14. Veksler D., Aniel F., Rumyantsev S. *et al.* GaN heterodimensional Schottky diode for THz detection, in: *SENSORS, IEEE*, 2006. P. 323–326. <https://doi.org/10.1109/ICSENS.2007.355471>.
15. Minkevicius L., Tamošiunas V., Kašalynas I. *et al.* Terahertz heterodyne imaging with InGaAs-based bow-tie diodes. *Appl. Phys. Lett.* 2011. **99**. P. 131101. <https://doi.org/10.1063/1.3641907>.
16. van Exter M., Fattinger C., Grischkowsky D. Terahertz time-domain spectroscopy of water vapor. *Opt. Lett.* 1989. **14**. P. 1128–1130. <https://doi.org/10.1364/OL.14.001128>.
17. van Exter M., Grischkowsky D. Carrier dynamics of electrons and holes in moderately doped silicon. *Phys. Rev. B.* 1990. **41**, No 17. P. 12140–12148. <https://doi.org/10.1103/PhysRevB.41.12140>.
18. Guo H.C., Zhang X.H., Liu W., Yong A.M., Tang S.H. Terahertz carrier dynamics and dielectric properties of GaN epilayers with different carrier concentrations. *J. Appl. Phys.* 2009. **106**. P. 063104. <https://doi.org/10.1063/1.3212966>.
19. Ulbricht R., Hendry E., Shan J., Heinz T.F., Bonn M. Carrier dynamics in semiconductors studied with time-resolved terahertz spectroscopy. *Rev. Mod. Phys.* 2011. **83**, No 2. P. 543–586. <https://doi.org/10.1103/RevModPhys.83.543>.
20. Lloyd-Hughes J., Jeon T.-I. A review of the terahertz conductivity of bulk and nano-materials. *J. Infrared Milli Terahz Waves.* 2012. **33**. P. 871–925. <https://doi.org/10.1007/s10762-012-9905-y>.
21. You D., Jones R.R., Bucksbaum P.H., Dykaar D.R. Generation of high-power sub-single-cycle 500-fs electromagnetic pulses. *Opt. Lett.* 1993. **18**, No 4. P. 290–292. <https://doi.org/10.1364/OL.18.000290>.
22. Kuehn W., Gaal P., Reimann K. *et al.* Terahertz-induced interband tunneling of electrons in GaAs. *Phys. Rev. B.* 2010. **82**. P. 075204. <https://doi.org/10.1103/PhysRevB.82.075204>.
23. Koroteyev V.V., Kochelap V.A., Kim K.W. Electron transport in bulk GaN under ultrashort high-electric field transient. *Semicond. Sci. Technol.* 2011. **26**. P. 105008. <https://doi.org/10.1088/0268-1242/26/10/105008>.
24. Zhao X., Zhang J., Fan K. *et al.* Nonlinear terahertz metamaterial perfect absorbers using GaAs [Invited]. *Photon. Res.* 2016. **4**, No 3. P. A16–A21. <https://doi.org/10.1364/PRJ.4.000A16>.
25. Yan B., Fang J., Qin S. *et al.* Experimental study of plasmon in a grating coupled graphene device with a resonant cavity. *Appl. Phys. Lett.* 2015. **107**. P. 191905. <https://doi.org/10.1063/1.4935344>.
26. Qin H., Yu Y., Li X. *et al.* Excitation of terahertz plasmon in two-dimensional electron gas. *Terahertz Science and Technology.* 2016. **9**, No 2. P. 71–81. <https://doi.org/10.11906/TST.71-81.2016.06.07>.
27. Koroteyev V., Lyaschuk Yu., Kochelap V. *et al.* Interaction of sub-terahertz radiation with low-doped grating-based AlGaIn/GaN plasmonic structures. Time-domain spectroscopy measurements and electrodynamic modeling. *SPQEO.* 2019. **22**. P. 237–251. <https://doi.org/10.15407/spqeo22.02.237>.
28. Pashnev D., Kaplas T., Korotieiev V. *et al.* Terahertz time-domain spectroscopy of two-dimensional plasmons in AlGaIn/GaN heterostructures. *Appl. Phys. Lett.* 2020. **117**, No 5. P. 051105. <https://doi.org/10.1063/5.0014977>.
29. Pashnev D., Koroteyev V., Janonis V. *et al.* Experimental evidence of temperature dependent effective mass in AlGaIn/GaN heterostructures observed via THz spectroscopy of 2D plasmons. *Appl. Phys. Lett.* 2020. **117**. P. 162101. <https://doi.org/10.1063/5.0022600>.
30. Otsuji T., Shur M. Terahertz plasmonics: Good results and great expectations. *IEEE Microwave Mag.* 2014. **15**. P. 43–50. <https://doi.org/10.1109/MMM.2014.2355712>.
31. Otsuji T., Karasawa H., Watanabe T. *et al.* Emission of terahertz radiation from two-dimensional electron systems in semiconductor nano-heterostructures. *C. R. Physique.* 2010. **11**. P. 421–432. <https://doi.org/10.1016/j.crhy.2010.04.002>.
32. Popov V.V., Fateev D.V., Otsuji T. *et al.* Plasmonic terahertz detection by a double-grating-gate field-effect transistor structure with an asymmetric unit cell. *Appl. Phys. Lett.* 2011. **99**. P. 243504. <https://doi.org/10.1063/1.3670321>.
33. Popov V.V. Plasmon excitation and plasmonic detection of terahertz radiation in the grating-gate field-effect-transistor structures. *J. Infrared Milli Terahz Waves.* 2011. **32**. P. 1178–1191. <https://doi.org/10.1007/s10762-011-9813-6>.
34. Lyaschuk Y.M., Koroteyev V.V. Theory of detection of terahertz radiation in hybrid plasmonic structures with drifting electron gas. *Ukr. J. Phys.* 2017. **62**, No 10. P. 889. <https://doi.org/10.15407/ujpe62.10.0889>.
35. Jessop D.S., Kindness S.J., Xiao L. *et al.* Graphene based plasmonic terahertz amplitude modulator operating above 100 MHz. *Appl. Phys. Lett.* 2016. **108**. P. 171101. <https://doi.org/10.1063/1.4947596>.
36. Mikhailov S.A. Plasma instability and amplification of electromagnetic waves in low-dimensional electron systems. *Phys. Rev. B* 1998. **58**. P. 1517. <https://doi.org/10.1103/PhysRevB.58.1517>.

37. Petrov A.S., Svintsov D., Ryzhii V., Shur M.S. Amplified-reflection plasmon instabilities in grating-gate plasmonic crystals. *Phys. Rev. B*. 2017. **95**. P. 045405. <https://doi.org/10.1103/PhysRevB.95.045405>.
38. Korotyeyev V.V., Kochelap V.A., Danylyuk S., Varani L. Spatial dispersion of the high-frequency conductivity of two-dimensional electron gas subjected to a high electric field: Collisionless case. *Appl. Phys. Lett.* 2018. **113**. P. 041102. <https://doi.org/10.1063/1.5041322>.
39. Korotyeyev V.V., Kochelap V.A. Plasma wave oscillations in a nonequilibrium two-dimensional electron gas: Electric field induced plasmon instability in the terahertz frequency range. *Phys. Rev. B*. 2020. **101**. P. 235420. <https://doi.org/10.1103/PhysRevB.101.235420>.
40. Withayachumnankul W., Naftaly M. Fundamentals of measurement in terahertz time-domain spectroscopy. *J Infrared Milli Terahz Waves*. 2014. **35**. P. 610–637. <https://doi.org/10.1007/s10762-013-0042-z>.
41. Jepsen U. Phase retrieval in terahertz time-domain measurements: a how to tutorial. *J. Infrared Milli Terahz Waves*. 2019. **40**. P. 395–411. <https://doi.org/10.1007/s10762-019-00578-0>.
42. Ding S.-H., Li Q., Li Y.-D., Wang Q. Continuous-wave terahertz digital holography by use of a pyroelectric array camera. *Opt. Lett.* 2011. **36**, No 11. P. 1993–1995. <https://doi.org/10.1364/OL.36.001993>.
43. Petrov N.V., Kulya M.S., Tsyppin A.N. *et al.* Application of terahertz pulse time-domain holography for phase imaging. *IEEE Trans. Terahertz Sci. Technol.* 2016. **6**, No 3. P. 464–471. <https://doi.org/10.1109/TTHZ.2016.2530938>.
44. Naftaly M., Molloy J.F., Magnusson B. *et al.* Silicon carbide – a high-transparency nonlinear material for THz applications. *Opt. Exp.* 2016. **24**, No 3. P. 2590. <https://doi.org/10.1364/OE.24.002590>.
45. Bechhoefer J. Kramers-Kronig, Bode, and the meaning of zero. *Am. J. Phys.* 2011. **79**. P. 1053–1059. <https://doi.org/10.1119/1.3614039>.
46. Fateev D.V., Popov V.V., Shur M.S. Plasmon spectra transformation in grating-gate transistor structure with spatially modulated two-dimensional electron channel. *Semiconductors*. 2010. **44**. P. 1455. <https://doi.org/10.1134/S1063782610110059>.
47. Schaich W.L. Analysis of a special model for a grating coupler. *Phys. Rev. B*. 2000. **62**, No 4. P. 2721–2730. <https://doi.org/10.1103/PhysRevB.62.2721>.
48. Lyaschuk Y.M., Korotyeyev V.V. Interaction of a terahertz electromagnetic wave with the plasmonic structure system grating-2D gas. Analysis of features of the near field. *Ukr. J. Phys.* 2014. **59**, No 5. P. 495–504. <https://doi.org/10.15407/ujpe59.05.0495>.
49. Muravjov A.V., Veksler D.B., Popov V.V. *et al.* Temperature dependence of plasmonic terahertz absorption in grating-gate gallium-nitride transistor structures. *Appl. Phys. Lett.* 2010. **96**. P. 042105. <https://doi.org/10.1063/1.3292019>.

Authors and CV



Dr. Vadym Korotyeyev born 1977 in Lutsk (Volyn region, Ukraine), graduated in physics in 1999, the PhD degree in solid state physics in 2006 from the V. Lashkaryov Institute of Semiconductor Physics, NAS of Ukraine. Since 2010, he is a senior researcher at the Department of Theoretical Physics at the same institute. He is the author of more than 20 publications. His main research activity is in the field of electronic transport in nanoscaled structures and THz optoelectronics. <https://orcid.org/0000-0002-0463-7872>



Dr. Yurii Lyaschuk born 1988 in Ostriv (Rivne region, Ukraine), graduated in physics in 2010 (Eastern European National University), the PhD degree in semiconductor physics in 2018 from the V. Lashkaryov Institute of Semiconductor Physics, NAS of Ukraine. Since 2016, he is a junior researcher at the Department of electrical and galvanomagnetic properties of semiconductors at the V. Lashkaryov Institute of Semiconductor Physics, NASU. He is the author of 17 publications. His main research activity is in the field of electrodynamics of low-dimensional systems, THz plasmonics and optoelectronics. <https://orcid.org/0000-0001-9112-3505>



Prof., Dr. Viacheslav A. Kochelap born 1944 in Kyiv (Ukraine), graduated in theoretical physics in 1966 (Kiev State University), the PhD degree in solid state physics in 1970 from the Institute of Semiconductor Physics, NAS of Ukraine. Since 1987, he is full Professor at the Department of Theoretical Physics, V. Lashkaryov Institute of Semiconductor Physics, NASU. He is the author of more than 250 publications. His main research activity is in the field of electronic transport, fluctuation phenomena and THz-physics of semiconductors and semiconductor nanoscale devices. <https://orcid.org/0000-0002-7181-0356>

Author's contribution

Lyaschuk Yu.M.: calculations, initial draft preparation, review & editing.

Korotyeyev V.V.: key ideas, calculations, validation, initial draft preparation, review & editing.

Kochelap V.A.: key ideas, conceptualization, validation, writing – review & editing, supervision.

Особливості амплітудних та фазових спектрів напівпровідникових структур у ТГц діапазоні частот

Ю.М. Ляшук, В.В. Коротєєв, В.О. Кочелап

Анотація. Розглянуто головні особливості амплітудних і фазових спектрів пропускання/відбивання декількох модельних напівпровідникових структур, у тому числі діелектричну підкладку, тонкий провідний шар, розміщений між двома діелектричними середовищами, тонкий провідний шар, розміщений на діелектричній підкладці, і гібридну плазмонну структуру з тонким провідним каналом під металевою ґраткою. Аналіз було здійснено з використанням аналітичних виразів, отриманих у результаті розв'язків рівнянь Максвелла при нормальному падінні плоскої електромагнітної хвилі. Показано, що специфічна поведінка амплітудних та фазових спектрів у ТГц діапазоні може бути використана для визначення базових параметрів 2D-електронного газу, включаючи концентрацію вільних електронів та їх рухливість, у рамках експериментальних методик ТГц спектроскопії з розділенням у часі. Нами запропоновано ефективний фазовий модулятор ТГц випромінювання з електричним контролем робочих параметрів, що ґрунтується на ефекті 2D-плазмонного резонансу в гібридних плазмонних структурах зі просторово-модульованим профілем концентрації у тонкому провідному шарі.

Ключові слова: фаза, фазовий спектр, ТГц спектроскопія з розділенням у часі, ТГц фазовий модулятор, плазмонна структура, металічна ґратка.